Catalysis Letters Vol. 107, Nos. 1–2, February 2006 (© 2006)
DOI: 10.1007/s10562-005-9726-x

Synthesis of Pd nanoparticles in La-doped mesoporous Titania with polycrystalline framework

Shuai Yuan[a], Qiaorong Sheng[a], Jinlong Zhang[a,*], Feng Chen[a], Masakazu Anpo[b], and Weilin Dai[c]

[a]*Lab for Advanced Materials and Institute of Fine Chemicals, East China University of Science and Technology, 130 Meilong Road, Shanghai 200237, P.R. China*

[b]*Departrnent of Applied Chemistry, Graduate School of Engineering, Osaka Prefecture University, 1–1 Gakuen-cho, Sakai, Osaka 599-8531, Japan*

[c]*Department of Chemistry, Fudan University, 200433, P.R. China*

Received 12 September 2005 Accepted 19 November 2005

A simple synthetic method to prepare highly dispersed Pd nanoparticles in La-doped mesoporous titania with polycrystalline framework by coassembly and photoreduction is reported. The mesoporous materials were characterized by thermogravimetric (TGA)/differential scanning calorimetric (DSC), low angle and wide angle X-ray diffraction (XRD), transmission electron microscope (TEM), high-resolution transmission electron microscopy (HRTEM) and N_2 adsorption–desorption. The photocatalytic activities of the prepared mesoporous materials were evaluated by the photodegradation of methyl orange.

KEY WORDS: Pd; photoreduction; mesoporous titania; polycrystalline framework.

1. Introduction

Noble metals, such as Pt, Pd and Au, are widely used as the catalysts in the fields of organic synthesis, petrochemistry, etc. Noble metal particles loaded on the substrates with large surface area have high dispersity and are convenient to be recycled. Anchoring noble metal nanoparticles or clusters in zeolites can combine the advantages of nanoparticles and micropores [1]. However, the micropore sizes less than 2 nm limit the applications of these pore systems to small molecules.

The discovery of mesoporous materials provided a new kind of supports to load nanoparticles with high dispersity [2]. The combination of noble metal nanoparticles with well ordered mesoporous materials is of interest in the field of catalysis, separation and sensors [3–8]. It is well known that the substrates not only provide spaces for nanoparticles, but also have great effects on catalytic activities. For example, anatase, rutile and brookite are three different crystal structures of TiO_2. Pd supported on different kind of titania crystals has various catalytic activity and selectivity [9]. Furthermore, the presence of rare earth could promote the catalytic activity of Pd nanoparticles supported on TiO_2 in the oxidation reaction [10].

To introduce Pd nanoparticles into rare earth doped mesoporous titania with highly crystallized walls and long-range ordered mesopores may bring more excellent properties in the redox reactions. However, it is difficult to introduce metal nanoparticles into mesopores by traditional impregnation methods, because they tend to deposit richly on outer surface of mesoporous materials. Moreover it is difficult to control the loading amount by impregnation. Many efforts have been done to solve these problems. For example, Zhu et al. [11] introduced Au nanoparticles into mesoporous silica by coassembly. Perez et al. [12] prepared 5 nm Au particles in amorphous titania by electrodeposition. Yu et al. [13] reported the formation of Au nanoclusters in mesoporous titania film by a modified impregnation methods with ultrasonic treatment in vacuum and photochemical reaction.

Based on our previous work [14], a simple and effective method is reported in this paper to prepare highly dispersed Pd nanoparticles in La-doped mesoporous titania with crystalline framework by coassembly and *in-situ* photoreduction. The precursor $PdCl_4^{2-}$, was added before the evaporation-induced self assembly (EISA) process, and was dispersed uniformly on the surface of titania colloid which was positively charged in acid condition, then titania colloid assembled to mesoporous material. Because Pd^{2+} has larger ionic radius than Ti^{4+} (0.086 and 0.061 nm respectively) [15], it is difficult for Pd^{2+} to be dissolved into crystal lattice of anatase. After calcination in air flow, highly dispersed PdO was formed on the surface of assembling units-anatase crystals. The polycrystalline walls generated electrons and holes under UV illumination, the photogenerated electrons could reduce PdO into Pd. Scheme 1 is an illustration of the process. In such a process, there is no loss of Pd except volatile matters and organic template. For comparison, the sample was also reduced by H_2 at 473 K.

* To whom correspondence should be addressed.
E-mail: jlzhang@ecust.edu.cn

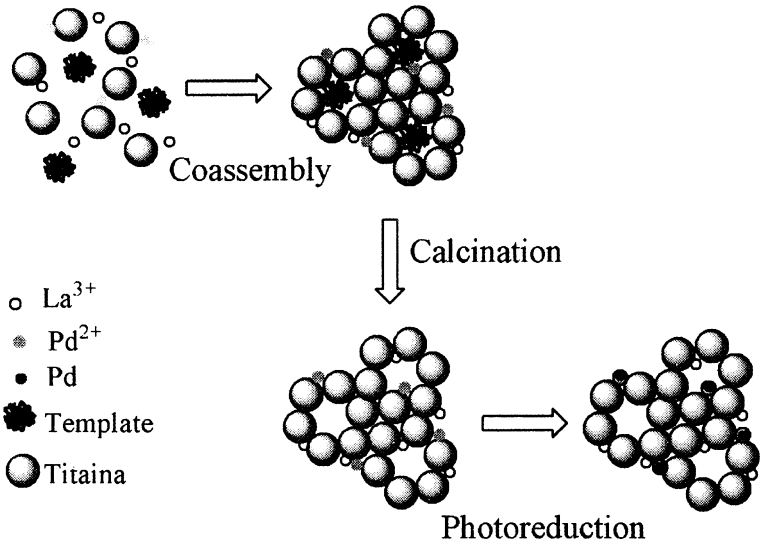

Scheme 1. Preparation of Pd nanoparticles in La-doped mesoporous titania by coassembly and *in-situ* photoreduction.

2. Experimental section

2.1. Chemicals and synthesis

In the synthesis process, 2.130 g Pluronic P-123 was dissolved in 7.000 g BuOH under vigorous stirring for 30 min. Then 0.054 g $La(NO_3)_3{\cdot}6H_2O$ and 5 g $Ti(OBu)_4$ were added into the P-123 solution, followed by stirring for an additional 60 min. In a test-tube 0.013 g $PdCl_2$ was dissolved in 2.250 g dilute hydrochloric acid (23.8 wt%). Then, the solution was added dropwise to the above mixture under stirring and ultrasonic treatment (59 kHz, 45 W). The temperature of ultrasonic cell was kept at 298 K. The molar ratio of Pd: La: P-123: HCl: H_2O: BuOH: Ti was kept 0.005: 0.01: 0.025: 1: 6.5: 6.5: 1. After 30 min, the transparent sol was transferred from the reactor to an open Petri dish. The sol extended sufficiently and formed a uniform thin layer. In the aging stage, the environmental humidity was kept at 75% in the first day. After aging at 298 K for 4 day, 413 K for 2 h and then 473 K for 2 h, the cracked-free thin layer was calcined at 673 K for 1 h in airflow. The brown powder, notated as PdO/LaMT, was divided into two portions. One portion was dispersed in aqueous solution of ethanol (1: 1, v/v), then illuminated at room temperature by UV light (300 W, I_{max} at 365 nm) for 0.5 h after saturated by N_2(99.99%) for 20 min. The black product was notated as Pd(P)/LaMT. The other portion was reduced in H_2 (99.99%) flow at 473 K for 4 h. H_2 flow was stopped until the sample was cooled down to room temperature. The black product was notated as Pd(H)/LaMT. The sample prepared in the same manner without Pd is noted as LaMT.

The photocatalytic activities of the prepared samples were evaluated from an analysis of the photodegradation of methyl orange. About 0.0400 g sample was ultrasonically dispersed in 40 ml methyl orange solution (20 mg l^{-1}). After stirring in dark for 60 min, the adsorption was balanced. The solutions were then irradiated with a UV source (300 W, I_{max} at 365 nm),The concentrations of solutions were detected 60 min later with a Cary 100 UV-visible spectrophotometer at 464 nm.

2.2. Characterization

Thermogravimetric (TGA)/differential scanning calorimetric (DSC) analysis (Instrument, NETZSCH STA 409 PC/PG) was performed in flowing oxygen (7 cm^3 min^{-1}) with a heating rate of 2.5 K min^{-1}. Low-angle X-ray diffraction (XRD) patterns of all samples were collected in $\theta - 2\theta$ mode using Rigaku D/MAX-2550 diffractometer ($CuK\alpha_1$ radiation, $\lambda = 1.5406$ Å), operated at 40 kV and 200 mA. Wide-angle XRD diagrams were collected in the same mode, but operated at 100 mA. The Pd particle size was estimated by applying the Scherrer equation to the FWHM of the (111) peak. The sample morphology was observed under transmission electron microscopy (TEM) and high-resolution transmission electron microscopy (HRTEM) on a 2100 JEOL microscope (200 kV) using copper grids. The instrument employed for XPS studies was Perkin Elmer PHI 5000C ESCA System with Al Kα radiation operated at 250 W. The porous texture of the powders was analyzed from nitrogen adsorption–desorption isotherms at 77 K. By using a Micromeritics ASAP 2000 system, the BET and BJH methods were applied for the determination of the specific surface area, and the mean mesopore equivalent diameter, respectively. These samples were outgassed overnight at 473 K before N_2 adsorption–desorption analysis.

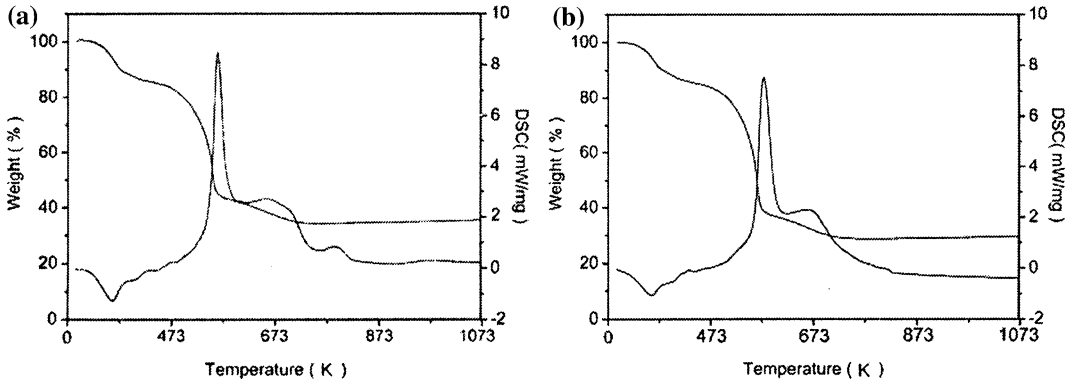

Figure 1. TGA–DSC curve of as-synthesized La-doped mesoporous organic–inorganic hybrid containing Pd^{2+} (a); TGA–DSC curve of as-synthesized La-doped mesoporous organic–inorganic hybrid containing no Pd^{2+} (b).

3. Results and discussion

The thermogravimetric curve presented in figure 1(a) shows a three-step weight loss pattern for as-synthesized mesoporous organic–inorganic hybrid containing Pd^{2+} and La^{3+}. The first step below 393 K is due to the loss of volatile species, such as water, butanol and HCl, which are endothermic reaction. The second step between 393 and 558 K is attributed to the decomposition of the P123 template. The third step of weight loss ranging from 558 to 693 K corresponds to the removal of residual organic compounds. Correspondingly, there are a sharp exothermic peak around 560 K and a low and broad exothermic peak around 673 K. The exothermic peak around 783 K without corresponding weight loss is caused by the phase transformation from anatase to rutile. However, in the TG-DSC figure of as-synthesized mesoporous titania without Pd^{2+} (figure 1(b)), the maximal exothermic peak is around 579 K. Moreover, there is no exothermic peak around 783 K.

The differences between two TG-DSC figures should be attributed to the presence and absence of Pd. The oxidation of organic compounds was catalyzed by Pd [16], which resulted in the shift of maximal exothermic peak to lower temperature. In figure 1(a), the exothermic peak around 783 K should be attributed to the phase transformation from anatase to rutile promoted by Pd^{2+}. La^{3+} and Pd^{2+} have larger ionic radius than Ti^{4+} (0.103, 0.086 and 0.061 nm respectively) [15]. So it is difficult for La^{3+} or Pd^{2+} to replace Ti^{4+} inside the anatase crystals. It is possible that La–O–Ti bonds and Pd–O–Ti bonds were formed on the surface of anatase crystals. Element with lower electronegativity than titanium, such as lanthanum, can improve the stability of titania crystals by enhancing the strength of Ti–O bonds [17]. On the contrary, element with higher electronegativity than titanium, such as palladium, seems to decrease the stability of titania crystals by weakening the strength of Ti–O bonds.

In figure 2, the appearance of low-angle diffraction peaks indicates that the mesostructure was preserved after calcination. Illumination by UV light in aqueous solution of ethanol or calcination in H_2 flow at 473 K did no damage to the mesostructure. From wide-angle XRD patterns, a series of peaks for anatase can be observed. After calcinations, characteristic peaks belonging to PdO are too weak to be confirmed. PdO particles may be very small and highly dispersed. Otherwise, the presence of a very small amount of PdO would display characteristic peaks in the wide-angle XRD pattern [18]. The PdO may exist on the outer

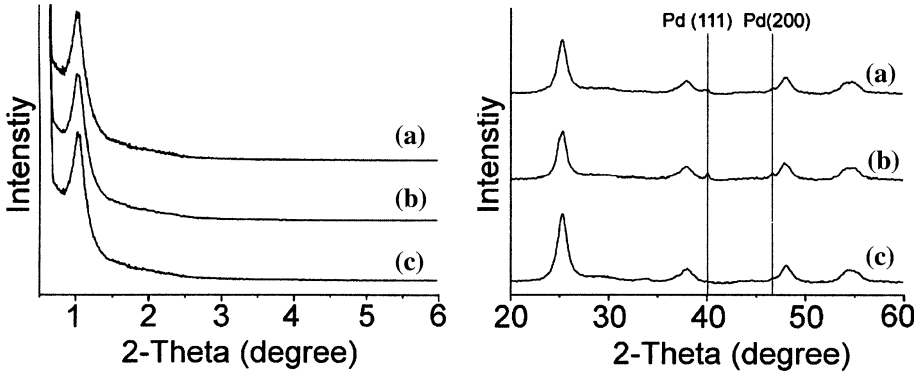

Figure 2. Low-angle XRD patterns (left) and wide angle XRD patterns (right) of Pd(P)/LaMT (a), Pd(H)/LaMT (b) and PdO/LaMT (c).

Table 1
Pore-wall parameters and Pd nanoparitcle sizes of Pd(P)/LaMT and Pd(H)/LaMT

Sample	d_{100} (nm)	S_{BET}[a]($m^2\ g^{-1}$)	D_{BJH}[b](nm)	$D_{Anatase}$[c](nm)	D_{Pd}[d](nm)
Pd(P)/LaMT	8.5	110	3.9	9.2	6
Pd(H)/LaMT	8.5	74	3.4	9.2	14

[a]BET surface area;
[b]Average pore diameter, estimated by using BJH model;
[c]Anatase particle size calculated by Scherrer equation;
[d]Pd particle size calculated by Scherrer equation.

surface, inner surface of mesoporous titania, or in the gaps between anatase nanoparticles. After thermal reduction by hydrogen at 473 K for 4 h, two peaks belonging to Pd (111) planes and (200) planes emerged in the XRD pattern of Pd(H)/LaMT [19]. In comparison with Pd(H)/LaMT, the peaks belonging to Pd (111) planes and (200) planes for Pd(P)/LaMT are weaker and broader, owing to smaller metal particle size and higher dispersity. The data of pore-wall parameters and Pd nanoparitcle sizes of Pd(P)/LaMT and Pd(H)/LaMT were summarized in table 1.

TEM and HRTEM images are shown in figure 3. The mesoporous titania matrix has long-range order and polycrystalline framework. There is no obvious agglomerate Pd particles in the mesopores of Pd(P)/LaMT (figure 3a, b). Illuminated by UV light at room temperature, PdO was reduced *in-situ* by photogenerated electrons in the presence of ethanol as photogenerated holes captor. The visible Pd nanoparticles in the TEM image of Pd(P)/LaMT (figure 3b) is about 5 nm. However, most Pd nanoparticles are difficult to be discerned on the pore-walls, because they are dissolved homogenously in the framework. In contrast, Pd nanoparticles with larger sizes can be observed in the TEM image of Pd(H)/LaMT (figure 3d, e). In the mesopores, the growth of Pd nanoparticles was restricted by the pore diameter. However, on the outer surface, it is easier for Pd nanoparticles to migrate and agglomerate. Some Pd particles are larger than 18 nm. From the HRTEM image of Pd(P)/LaMT(figure 3c) and Pd(H)/LaMT(figure 3f), anatase (101) planes with $d = 0.35$ nm, Pd (111) planes with $d = 0.22$ nm and Pd (200) planes with $d = 0.19$ nm can be observed. Before reduction, the sintering of PdO was slow because of the strong chemical interaction with titania by forming Pd–O–Ti bonds. After reduction, Pd agglomerated to reduce surface energy, because high temperature accelerated the agglomeration of Pd, Pd nanoparticles prepared by hydrogen reduction at 473 K are larger than the ones prepared by photoreduction.

The valence states of palladium were analyzed by XPS spectra. Palladium only has one chemical state in

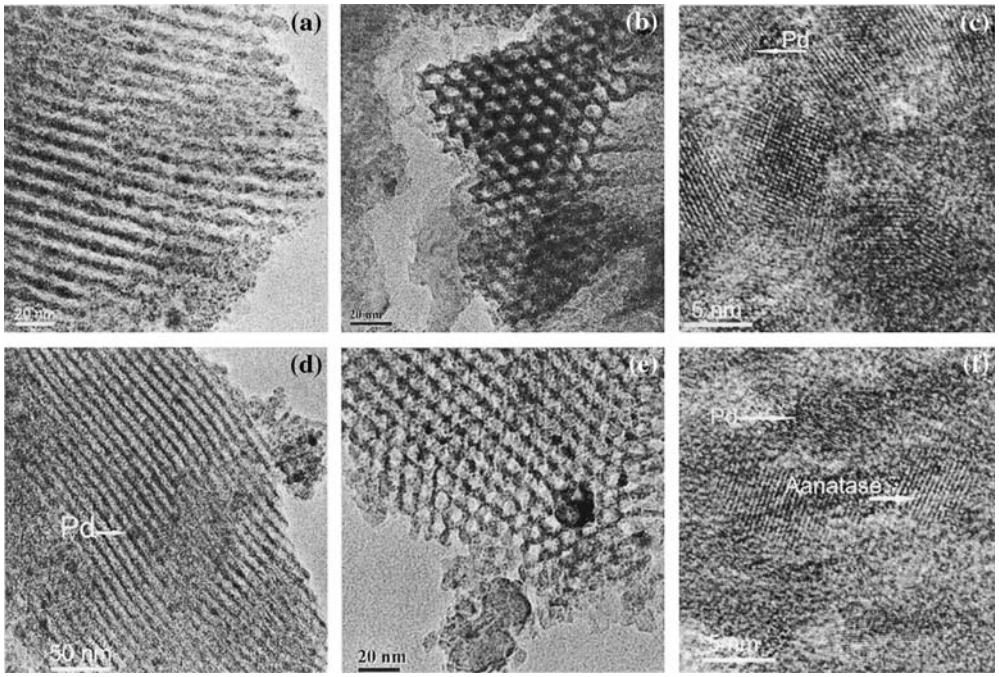

Figure 3. TEM images of Pd(p)/LaMT along the [110] direction (a) and [001] direction (b); (c) HRTEM of Pd(P)/LaMT along the [110] direction (d)and [001] direction (e); (f) HRTEM of Pd (H)/laMT.

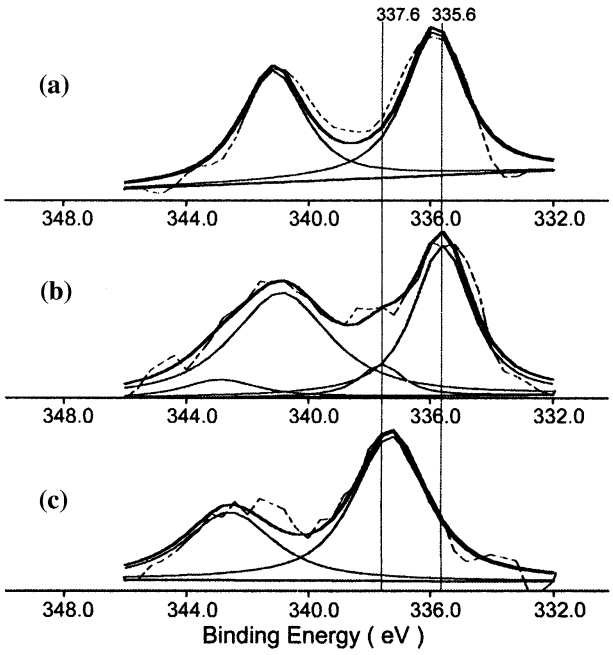

Figure 4. Pd 3*d* XPS spectra of Pd (p)/LaMT (a), Pd (H)/LaMT (b) and PdO/LaMT(c). The dashed lines are the measured data. The thick solid lines are the fitted data. The thin solid lines are the deconvoluted spectra.

Pd(P)/LaMT (figure 4a), which indicates the reduction was complete. The dispersion and the particles size of Pd^0 will affect the Pd $3d_{5/2}$ binding energy values greatly [20]. The Pd^0 $3d_{5/2}$ binding energy of Pd(P)/LaMT is 335.8 eV, 0.2 eV higher than that of Pd(H)/LaMT, which may be due to higher dispersion and smaller size of Pd nanoparticles. In contrast, two chemical states of palladium can be discerned in the XPS spectra of Pd(H)/LaMT (figure 4b). Pd $3d_{5/2}$ binding energies of 335.6 and 337.6 eV are attributed to Pd^0 and Pd^{2+}, respectively [5,21]. By quantitative analysis, there is about 14% residual PdO.

Figure 5 shows the binding energies of La 3d photoelectron peaks at 836,3 eV for La $3d_{5/2}$ line [22], which indicates that the chemical state of lanthanum is La^{3+} oxidation state before and after the reduction of Pd^{2+} by photogeneraged electrons or hydrogen. The conduction band edge of anatase, E_{cb} (-0.5 V_{NHE}, volts vs. normal hydrogen electrode) [13], is more negative than the redox potential of Pd^{2+}/Pd ($E(Pd^{2+}/Pd) = 0.915$ V_{NHE}) and more positive than the redox potential of La^{3+}/La ($E(La^{3+}/La) = -2.38$ V_{NHE}) [15]. So La^{3+} could not be reduced by photogenerated electrons. The photoreduction process may be represented by the following reactions [13]:

$$TiO_2 + h\nu \rightarrow h^+_{vb} + e^-_{cb} \quad (1)$$

$$C_2H_5OH + 2O_2 + 4h^+_{vb} \rightarrow 2CO_2 + H_2O + 4H^+ \quad (2)$$

$$Pd^{2+} + 2e^-_{cb} \rightarrow Pd^0 \quad (3)$$

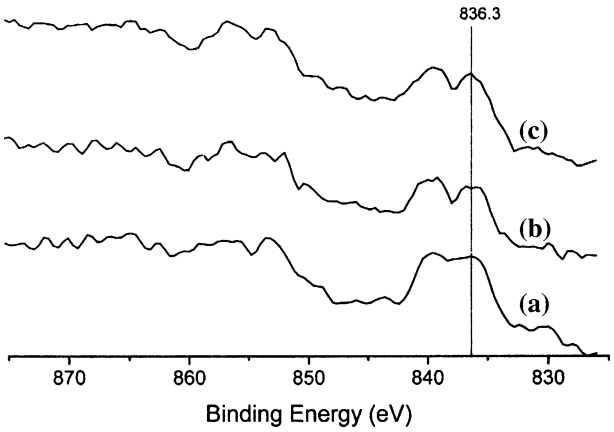

Figure 5. La 3*d* XPS spectra of Pd(P)/LaMT (a), Pd(H)/LaMT (b) and PdO/LaMT (c).

$$La^{3+} + 3e^-_{cb} \rightarrow La^0 \quad (4)$$

The results of specific surface area analysis are displayed in figure 6. The prepared materials have type IV gas adsorption isotherm, which is representative of materials containing large mesoporous channels [23,24]. The hysteresis loops have more type H1 characteristics than type H2, which indicates that the samples still reserve the uniform cylindrical mesopores. After reduced by photoreduction, the specific area is 110 m^2 g^{-1}. The average pore diameter estimated by using BJH model is 3.9 nm. The sample Pd(H)/LaMT has less specific surface area (74 m^2 g^{-1}) and smaller pore size (3.4 nm). High temperature will accelerate the sintering of Pd nanoparicles, which may be the main factor results in the less specific surface area and smaller pore diameter.

The photocatalytic activities of the composite materials of Pd nanoparticles and La-doped mesoporous titania prepared by photoreduction and hydrogen reduction were evaluated by the photodegradation of methyl orange. Pd(P)/LaMT has higher photocatalytic activity than LaMT and Pd(H)/LaMT (figure 7). Previous article reported that the morphology or geometrical factor of noble metal nanoparticles deposited on titania didn't affect photocatalytic properties as greatly as loading amount [25]. However, in the case of same loading amount, smaller noble metal nanoparitcle size will result in larger area contacting with titania which facilitates the separation of photogenerated electrons and holes.

4. Conclusions

A simple method is reported to synthesize highly dispersed Pd nanoparticles in La-doped mesoporous titania with crystallized walls by photoreducing PdO *in-situ* at room temperature. The loading amount of Pd is easy to control, because there is no loss of Pd in such

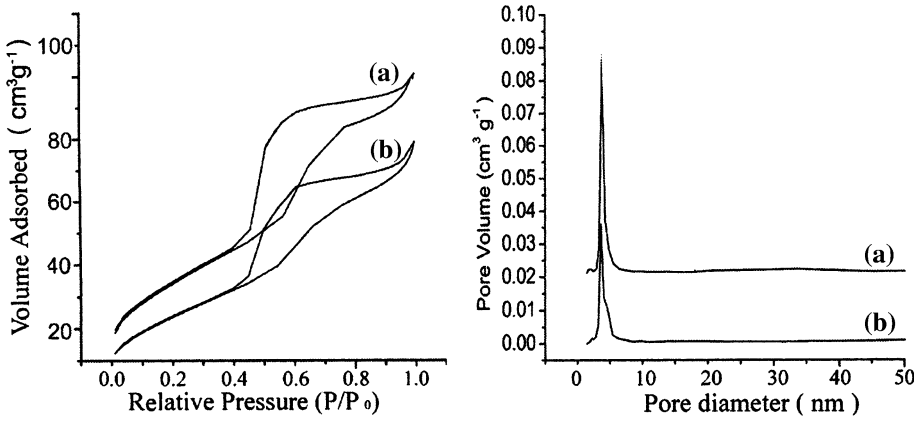

Figure 6. N_2 adsorption–desorption isotherms (left) and BJH pore size distribution plot (right) of Pd(p)/LaMT (a) pd(H)/LaMT (b).

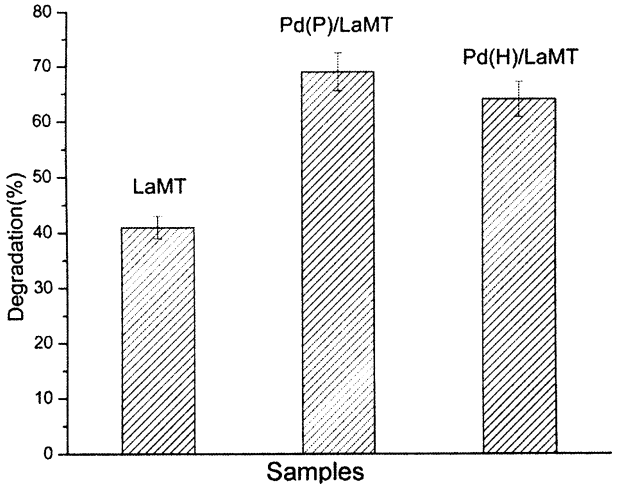

Figure 7. Photocatalytic activity of samples (Pd(P)/LaMT, Pd(P)/LaMT) and LaMT) evaluated by the degradation of methyl orange solution illuminated by a UV source for 60 min.

process. Compared with reduction by H_2, photoreduction is highly efficient and complete with high dispersion, which profits from the polycrystalline framework of mesoporous titania. The sample prepared by photoreduction has higher photocatalytic activity than that prepared by hydrogen reduction.

Acknowledgment

This work has been supported by Program for New Century Excellent Talents in University (NCET-04-0414); the National Basic Research Program of China (2004CB719500); Shanghai Nanotechnology Promotion Center (0452nm010), the Natural Science Foundation of China (20577009).

References

[1] J.G. Kim, S.K. Ihm, J.Y. Lee and R. Ryoo, J. Phys. Chem. 95 (1991) 8546.
[2] C.T. Kresge, M.E. Leonowicz, W.J. Roth, J.C. Vartuli and J.S. Beck, Nature 359 (1992) 710.
[3] R.C. Hayward, P. Alberius-Henning, B.F. Chmelka and G.D. Stucky, Microporous Mesoporous Mater. 44–45 (2001) 619.
[4] H.-R. Chen, J.-L. Shi, Y.-S. Li, J.-N. Yan, Z.-L. Hua, H.-G. Chen and D.-S. Yan, Adv. Mater. 15 (2003) 1078.
[5] I. Yuranov, L. Kiwi-Minsker, P. Buffat and A. Renken, Chem. Mater. 16 (2004) 760.
[6] A. Fukuoka, H. Araki, J. Kimura, Y. Sakamoto, T. Higuchi, N. Sugimoto, S. Inagaki and M. Ichikawa, J. Mater. Chem. 14 (2004) 752.
[7] J. Zhu, Z. Konya, V.F. Puntes, I. Kiricsi, C.X. Miao, J.W. Ager, A.P. Alivisatos and G.A. Somorjai, Langmuir 19 (2003) 4396.
[8] L.M. Bronstein, D.M. Chernyshov, R. Karlinsey, J.W. Zwanziger, V.G. Matveeva, E.M. Sulman, G.N. Demidenko, H.-P. Hentze and M. Antonietti, Chem. Mater. 15 (2003) 2623.
[9] É. Sípos, G. Farkas, A. Tungler and J.L. Figueiredo, J. Mol. Catal. A Chem. 179 (2002) 107.
[10] H. Zhu, Z. Qin, W. Shan, W. Shen and J. Wang, J. Catal. 225 (2004) 267.
[11] H. Zhu, B. Lee, S. Dai and S.H. Overbury, Langmuir 19 (2003) 3974.
[12] M.D. Pérez, E. Otal, S.A. Bilmes, G.J.A.A. de Soler-Illia, E.L. Crepaldi, D. Grosso and C. Sanchez, Langmuir 20 (2004) 6879.
[13] J.C. Yu, X. Wang, L. Wu, W. Ho, L. Zhang and G. Zhou, Adv. Funct. Mater. 14 (2004) 1178.
[14] S. Yuan, Q. Sheng, J. Zhang, F. Chen, M. Anpo and Q. Zhang, Microporous Mesoporous Mater. 79 (2005) 93.
[15] J.A. Dean, *Lange's Handbook of Chemistry* 15 ed. (McGraw-Hill, New York, 1999).
[16] P. Gélin and M. Primet, Appl. Catal. B 39 (2002) 1.
[17] C.P. Sibu, S.R. Kumar, P. Mukundan and K.G. Warrier, Chem. Mater. 14 (2002) 2876.
[18] J. Araña, J.M. Doña-Rodríguez, O. González-Díaz, E.T. Rendón, J.A. Herrera Melián, G. Colón, J.A. Navío and J.P. Peña, J. Mol. Catal. A: Chem. 215 (2004) 153.
[19] S.-W. Kim, J. Park, Y. Jang, Y. Chung, S. Hwang and T. Hyeon, Nano. Lett. 3 (2003) 1289.
[20] R. Díaz-Ayala, L. Arroyo, R. Raptis and C.R. Cabrera, Langmuir 20 (2004) 8329.
[21] K. Sun, W. Lu, M. Wang and X. Xu, Appl. Catal. A 268 (2004) 107.
[22] B.M. Reddy, P.M. Sreekanth, E.P. Reddy, Y. Yamada, Q. Xu, H. Sakurai and T. Kobayashi, J. Phys. Chem. B 106 (2002) 5695.
[23] P. Yang, D. Zhao, D.I. Margolese, B.F. Chmelka and G.D. Stucky, Chem. Mater. 11 (1999) 2813.
[24] M. Kruk and M. Jaroniec, Chem. Mater. 13 (2001) 3169.
[25] A.L. Linsebigler, G. Lu and J.T. Yates Jr., Chem. Rev. 95 (1995) 735.